Photo-isomerization fronts in dye-doped nematic liquid crystals

V. Odent,[1,*] M. G. Clerc,[1] C. Falcón,[1] U. Bortolozzo,[2] E. Louvergneaux,[3] and S. Residori[2]

[1]*Departamento de Física, Facultad de Ciencias Físicas y Matematicas, Universidad de Chile, Casilla 487-3, Santiago, Chile*

[2]*INLN, Université de Nice-Sophia Antipolis, CNRS, 1361 route des Lucioles, 06560 Valbonne, France*

[3]*Université Lille1, Laboratoire de Physique des Lasers, Atomes et Molécules, CNRS UMR 8523, 59655 Villeneuve d'Ascq Cedex, France*

**Corresponding author: vodent@ing.uchile.cl*

Received November 18, 2013; revised January 27, 2014; accepted February 14, 2014;
posted February 26, 2014 (Doc. ID 200899); published March 21, 2014

An experimental study of the photo-isomerization dynamics in dye-doped nematic crystals is reported, which shows that, when the sample is illuminated by a Gaussian beam, and for high enough input power, a transition from the nematic to the isotropic phase takes place in the illuminated area. The two phases are spatially connected via a front propagating outward from the center of the beam and following the local intensity profile and thus inducing a photo-controlled optical aperture. The optical intensity and temperature fields on the sample follow the same dynamical profile. The front dynamics is described by a phenomenological bi-stable model with an inhomogeneous control parameter, directly related to the beam intensity profile.

OCIS codes: (190.4420) Nonlinear optics, transverse effects in; (160.3710) Liquid crystals; (260.5130) Photochemistry.
http://dx.doi.org/10.1364/OL.39.001861

Optical nonlinearities have played an important role in the development of photonics since its origins. In particular, nonlinear effects in soft matter media, as nematic liquid crystals (LCs) [1], are quite attractive because of the large availability of these media, their widespread use, and the high level reached for their technological handling. One of the main optical properties of nematic LCs is their large birefringence, which can be modulated under the application of low ac voltages, hence, allowing strong enhancement of the optical contrast in imaging and display applications [2]. When dealing with nonlinear optics, the analogous of the optical Kerr effect can be obtained because of self-induced molecular reorientation [3,4]. Even though nonlinear effects in pure nematics require high-input powers, hence, reducing their applicability in practical opto-electronic devices, the addition of a small amount of certain types of dyes strongly reduces this requirement [5]. Especially when nematics are doped with azo-dyes, their nonlinear response to opto-electrical perturbations is increased by several orders of magnitude [6]. In this case, the dyes undergo a photo-isomerization transition; that is, molecular conformational changes are induced by the light [7], leading to local changes of molecular interactions and, thus, facilitating order–disorder transitions [8] and director realignment [9]. The fact that dye-doped liquid crystals (LCs) exhibit strong nonlinear effects allows these materials to be used for several applications, such as optical switching [8,10], real-time holography [11], image storage [12], transverse pattern formation [13], image processing [14], wave mixing [15], phase conjugation [16], and slow light [17]. Although photo-isomerization processes have been studied in different types of liquid crystalline structures [7–9,11], a characterization of the spatiotemporal dynamics associated to this type of optically induced phase transition is still lacking.

In this Letter, we present a study of the photo-isomerization-induced front propagation in a dye-doped nematic LC illuminated by a laser beam with a Gaussian profile. We show that, for high enough input power, a phase transition from the nematic to the isotropic state takes place in the illuminated area and that the two phases are spatially connected via a front propagating outward from the center of the beam. We measure the optical intensity over the LC sample and, thus, the local position of the front core. The temperature field over the sample closely follows the intensity profile, showing that the photochemical transition of the dye-doped LC is directly related to the light excitation. Using a phenomenological bi-stable model, which takes into account the inhomogeneous profile of the optical forcing, we characterize the front dynamics and its equilibrium states, showing that an effective optically controlled aperture can be established in the sample.

The experimental setup is depicted in Fig. 1(a). A dye-doped nematic liquid crystal cell (DDLC) is subjected to a Gaussian light beam. The LCLC consists of E7 nematic doped with an azo-dye (Methyl Red, concentration ∼0.5% by weight). The mixture is injected between two polyvinyl alcohol-coated glass plates with $d = 25$ μm thick spacers, with a planar anchoring of the LC molecules (nematic director $\vec{n}$ parallel to the confining walls). The system is irradiated by a frequency doubled Nd^{3+}:YVO_4 laser ($\lambda_0 = 532$ nm), vertically polarized [following the y axis, see Fig. 1(a)]. Two plano-convex lenses L_1 and L_2 increase the laser beam diameter ($2w$). The nematic director, in the (x, y) plane, is oriented at 45° with respect to the input beam polarization (along the y axis). A linear polarizer PL (following the x axis) is positioned at the output of the sample, perpendicular to the laser beam polarization. This configuration maximizes the contrast between the two phases. The transmitted beam is monitored by a CCD camera (Thorlabs DCU224M, 1280×1024 pixels). The thermal profile of the DDLC is also available through a far-infrared thermal camera (TC) (FLIR E45, 160×120 pixels). Images were acquired at 1 fps. The control parameter is the laser beam intensity I_0 via its power P_0 and its Gaussian beam size w.

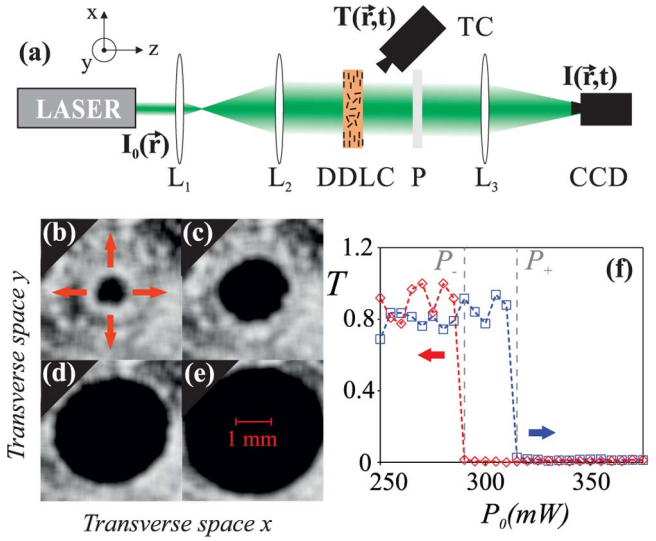

Fig. 1. Photo-controlled optical aperture. (a) Schematic sketch of the experimental setup. L_1 and L_2, plano-convex lenses; DDLC, dye-doped liquid crystal cell; P, polarizer along x axis; L_3, imaging lens; TC:, infrared thermal camera; CCD, CCD camera. (b)–(e) Experimental smoothed snapshots for $P_0 = 350$ mW and $w = 3.4$ mm ($I_0 = 1.93$ W/cm^2) at 55, 65, 125, and 500 s, respectively. (f) Sample transmissivity T as a function of the input power P_0: □ P_0 increasing and ◇ P_0 decreasing.

We focus on the photo-isomerization process driven by P_0. By increasing P_0 from 5 to 350 mW, a circular front develops in the inner region of the light beam, creating a dark disc, or optical aperture [see Fig. 1(b)]. The disc diameter increases in the transient regime with a decreasing speed [see Figs. 1(b)–1(d)] and becomes stationary at the end [see Fig. 1(e)]. The light extinction in the disc is a signature of the isotropic state, which is surrounded by the nematic phase. Indeed, in the illuminated area, the photo-isomerization of the dyes induces a phase transition to the isotropic state. The nature of this transition is of first order type, and the system exhibits a region of coexistence between two stable states: namely, the nematic and the isotropic phases. Notice that, without any external forcing, and at room temperature, the sample is in the nematic phase, and the clearing point for the LC used in our mixture, is $\theta_c \sim 58°$C.

We attribute the origin of the observed isotropic state to the LC reorientation without privileged direction. Indeed, the photo-isomerization process induced by interaction between the light and the disordered Methyl Red molecules, causes a random reorientation of the LC molecules [5,8,18]. The observed front is the result of the Gaussian profile of the light beam impinging on the sample. As the intensity is higher in the center, the transition starts at the center of the illuminated region; then, the isotropic state invades the nematic one. The front stops when these two phases are energetically equivalent [19]. This equilibrium corresponds to the so-called Maxwell point [20,21]. Figure 1(f) shows the hysteresis loop characterizing the transition. It depicts the sample transmissivity T [measured after the analyzer PL, see Fig. 1(a)] when P_0 is varied from 250 to 375 mW (I_0 from 1.38 to 2.06 W/cm^2). We change the power value every 10 min, an interval much larger than the LC relaxation time and, for every power, we record the final state. On the decreasing part of the loop, the isotropic phase ($T = 0$) appears for $P_+ = 315$ mW, whereas on the increasing part of the loop, the isotropic phase disappears for $P_- = 285$ mW. Note that the sample transmissivity is an adequate order parameter that characterizes the transition, showing the bi-stable loop between the two phases. It is well-known that the nematic–isotropic transition is of first order [22].

The transition can be described analytically by considering a phenomenological one-dimensional bi-stable model in inhomogeneous media [23–25]:

$$\frac{\partial u}{\partial t} = \eta(x) + u - u^3 + \frac{\partial^2 u}{\partial x^2}, \tag{1}$$

where $u(x,t)$ is the order parameter [26], which describes the phase state of the sample ($u \approx -1$ for the nematic phase, $u \approx +1$ for the isotropic phase) and $\eta(x) \equiv \alpha(-\sqrt{P_{\mathrm{Max}}} + \sqrt{P_0}e^{-(x/w)^2})$ is an *inhomogeneous bifurcation parameter* that accounts for the external forcing. Here, P_{Max} is the power at the Maxwell point and α is a calibration parameter. The front is a natural solution of Eq. (1), whose core position $x_0(t)$ is well-described by a hyperbolic tangent function in time $x_0(t) = a\tanh(b(t - t_0)$, where a, b, and t_0 depend of the experimental parameters [25]. We have tracked $x_0(t)$ by following the edge of the light extinction disc described above and by using the generalized Hough-transform [27]. The spatiotemporal diagram of the transmissivity T, taken along the horizontal diametrical line across the aperture corresponding to the sequence of Figs. 1(b)–1(e), is plotted in Fig. 2, together with the corresponding front core location $x_0(t)$. The experimental points are well-fitted with the hyperbolic tangent function by a nonlinear least squares method [cf. Fig. 2(b)], showing a good agreement between the experimental data and analytical findings.

The front connecting the nematic and isotropic states is motionless at the Maxwell point, which corresponds to impose $\eta(x_0) = 0$. Therefore, we can express the final front position x_0 as

$$2\left(\frac{x_0}{w}\right)^2 = \ln(P_0) - \ln(P_{\mathrm{Max}}). \tag{2}$$

Geometrically, one can determine P_{Max} through the following procedure: plot x_0^2 versus $\ln(P_0)$ and determine the intercept point [cf. Eq. (2)]. We performed numerical simulations of the bi-stable model (1) under a Gaussian forcing for different P_0 values. The final front position versus P_0 is plotted in Fig. 2(c), together with the expression of Eq. (2). We observe a good agreement between these two curves. The inferred Maxwell point is found to be equal to the analytical Maxwell point ($P_{\mathrm{Max}} = 0.09$). Experimentally, the same procedure is applied to determine the Maxwell point. The experimental final front positions are also fitted with a linear function as in the numerical part, giving $P_{\mathrm{Max}} = 280$ mW [see Fig. 2(c)]. Therefore, this value determines the minimal power needed to observe the phase transition. Note that, even though model (1) is a phenomenological one, it enables us to appropriately predict the final front position as a

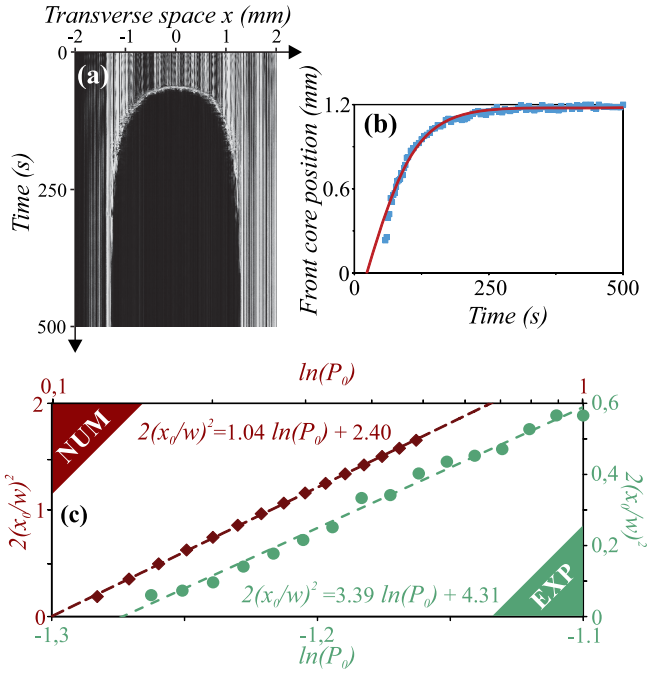

Fig. 2. One-dimensional characterization of the optical aperture dilation. (a) Spatiotemporal evolution of the transmissivity T taken along the horizontal diametrical line across the aperture of Figs. 1(b)–1(e), where $x = 0$ corresponds to the center of the Gaussian beam forcing the DDLC sample. (b) Evolution of the front core position: ■ experimental points, – fit using the hyperbolic tangent function derived from model (1). (c) Final front position as a function of P_0: ◆ numerical points, – numerical fit, • experimental points, – experimental fit. $w_{\text{num}} = 90$, $w_{\text{exp}} = 3.4$ mm.

function of the main parameter of the illuminating beam; namely, its intensity (through its power and its beam diameter). These features allow potential exploitations of the photo-controlled nematic-to-isotropic transition, for instance, realizing optically controlled and variable apertures or electro-optical apertures.

To characterize the spatial features of the phase transition, we have studied, simultaneously, the transmitted intensity and thermal fields $I(\vec{r}, t)$ and $\theta(\vec{r}, t)$, which are, respectively, the light intensity recorded by the CCD camera and the temperature recorded by the thermal camera TC [see Fig. 1(a)]. As the cameras do not have the same orientations in the experimental setup, we have rescaled the TC recording to get the same spatial resolution as for the CCD camera. Figure 3(a) shows an iso-surface plot of the CCD camera for $I(\vec{r}, t) = 25$ in gray scale and, in Fig. 3(b), an iso-surface plot of the thermal camera for $\theta(\vec{r}, t) = 36$°C. The spatial temperature profile, visible on the transverse cuttings [see Fig. 3(b)], also has a Gaussian dependence like the laser beam profile, as predicted in material absorption studies [28]. This shows clearly that the optical power and the temperature profiles are closely related fields in the photo-isomerization transition. However, the temperature values found in the sample are quite far from the critical temperature θ_c expected for the pure E7. These observations suggest that the photo-induced conformational changes of the azo-dyes are able to induce deformations of the nematic

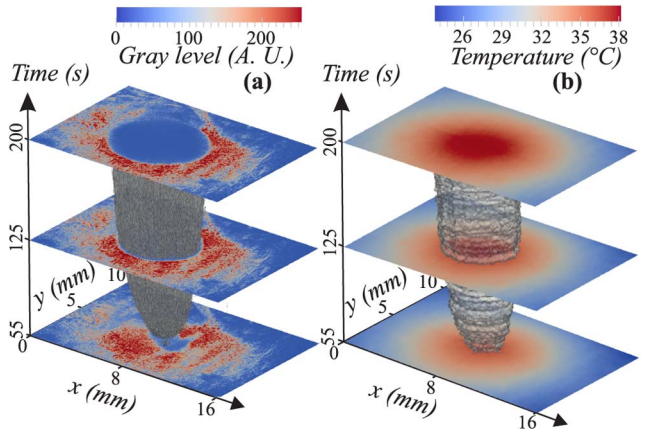

Fig. 3. Two-dimensional characterization of the aperture dilation. (a) Optical aperture: iso-surface for $I(\vec{r}, t) = 25$ (gray level) recorded with the CCD camera. (b) Thermal aperture: iso-surface for $\theta(\vec{r}, t) = 36°$ recorded with the thermal camera ($P_0 = 1$ W, $w = 5.5$ mm).

texture large enough for the transition to the isotropic state to occur at a much lower temperature.

The fundamental role of the photo-isomerization process in inducing the nematic-to-isotropic phase transition is confirmed by the dependence of the optical power threshold on the dye dopant concentration. This was measured by comparing the behavior of two samples with, respectively, 1% and 0.5% azo-dyes. For 0.25% and 0%, we did not observe the transition for the available maximum laser power. The results are shown in Fig. 4, where the two squares mark the respective phase transition points and the continuous lines delimit the region of stability of the nematic phase. Therefore, the dye concentration is a parameter controlling the aperture dilation at equivalent input power. Moreover, at equivalent dye concentrations, we observed the same phenomena also for different anchoring of the LC samples, either homeotropic or twisted.

In summary, we have shown that the photo-isomerization process in dye-doped nematic LCs enables the creation of a photo-controlled optical aperture when

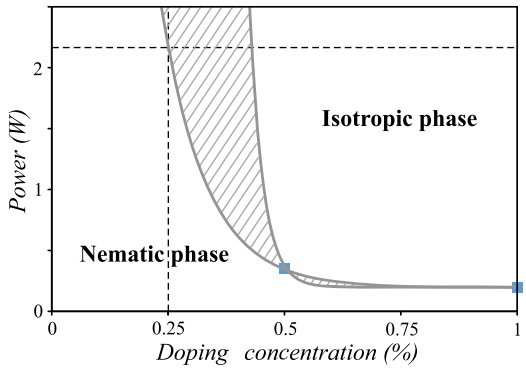

Fig. 4. Schematic phase diagram of nematic–isotropic phase transition. Optical power needed for the photo-isomerization induced nematic-to-isotropic transition to occur as a function of the dye dopant concentration; squares are experimental measurements corresponding to phase transitions, the dark region represents the transition zone between the nematic and the isotropic phases ($w = 3.4$ mm).

the sample is illuminated by a Gaussian beam. The aperture dilation process is understood in terms of the propagation of a front connecting the isotropic to the nematic phase. Indeed, due to the inhomogeneous beam profile, a front connection between the two phases can be achieved, as the isotropic state develops at the center of the beam, surrounded by the nematic one. The dilation process of the optical aperture is correlated with the temperature field inside the sample, which follows the light intensity profile. Using a phenomenological bi-stable model, with an inhomogeneous control parameter, we describe the dynamics of the system, which is in a quite good qualitative agreement with the experimental data. Such a photo-controlled phase transition could be used in practical device applications, as optically controlled and variable apertures.

We acknowledge financial support of the ANR international program, Project No. ANR-2010-INTB-402-02 (ANR-CONICYT 39), "COLORS." M. G. C., C. F., and V. O. thank for the financial support of FONDECYT projects 1120320, 1130354, and 3130382, respectively.

References

1. I. C. Khoo, *Liquid Crystals*, 2nd ed. (Wiley, 2007).
2. P. Yeh and C. Gu, *Optics of Liquid Crystal Displays* (Wiley, 1990).
3. N. V. Tabiryan, A. V. Sukhov, and B. Ya. Zel'dovich, Mol. Cryst. Liq. Cryst. **136**, 1 (1986).
4. I. C. Khoo, Phys. Rep. **471**, 221 (2009).
5. I. Jánossy and A. D. Lloyd, Mol. Cryst. Liq. Cryst. **203**, 77 (1991).
6. I. C. Khoo, S. Slussarenko, B. D. Guenther, M. Y. Shih, P. Chen, and W. V. Wood, Opt. Lett. **23**, 253 (1998).
7. I. Jánossy and L. Szabados, J. Nonlinear Opt. Phys. **7**, 539 (1998).
8. A. Shishido, O. Tsutsumi, A. Kanazawa, T. Shiono, T. Ikeda, and N. Tamai, J. Am. Chem. Soc. **119**, 7791 (1997).
9. A. G.-S. Chen and D. J. Brady, Opt. Lett. **17**, 1231 (1992).
10. S. M. Morris, M. M. Qasim, K. T. Cheng, F. Castles, D.-H. Ko, D. J. Gardiner, S. Nosheen, T. D. Wilkinson, H. J. Coles, C. Burgess, and L. Hill, Appl. Phys. Lett. **103**, 101105 (2013).
11. A. G. Chen and D. J. Brady, Opt. Lett. **17**, 441 (1992).
12. T. Ikeda and O. Tsutsumi, Science **268**, 1873 (1995).
13. S. G. Lukishova, N. Lepeshkin, R. W. Boyd, and K. L. Marshall, Mol. Cryst. Liq. Cryst. **453**, 393 (2006).
14. M. Y. Shih, A. Shishido, P. H. Chen, M. V. Wood, and I. C. Khoo, Opt. Lett. **25**, 978 (2000).
15. D. Wei, A. Iljin, Z. Cai, S. Residori, and U. Bortolozzo, Opt. Lett. **37**, 734 (2012).
16. D. Wei, S. Residori, and U. Bortolozzo, Opt. Lett. **37**, 4684 (2012).
17. D. Wei, U. Bortolozzo, J. P. Huignard, and S. Residori, Opt. Express **21**, 19544 (2013).
18. L. Ziyang, J. Shi, X. Ying, L. P. Shi, W. Jian, Z. X. Liang, and Z. R. Qiu, Phys. Lett. A **270**, 326 (2000).
19. Y. Pomeau, Physica D **23**, 3 (1986).
20. R. E. Goldstein, G. H. Gunaratne, L. Gil, and P. Coullet, Phys. Rev. A **43**, 6700 (1991).
21. M. G. Clerc, S. Residori, and C. S. Riera, Phys. Rev. E **63**, 060701(R) (2001).
22. S. Chandrasekhar and N. V. Madhusudana, Appl. Spectrosc. Rev. **6**, 189 (1972).
23. F. Haudin, R. G. Elías, R. G. Rojas, U. Bortolozzo, M. G. Clerc, and S. Residori, Phys. Rev. Lett. **103**, 128003 (2009).
24. F. Haudin, R. G. Elías, R. G. Rojas, U. Bortolozzo, M. G. Clerc, and S. Residori, Phys. Rev. E **81**, 056203 (2010).
25. V. Odent, "Localisation spatiale de la lumière dans des systèmes à cristaux liquides," Ph.D. thesis (Université de Lille 1, 2012), http://www.theses.fr/2012LIL10046.
26. L. D. Landau and E. M. Lifshitz, *Statistical Physics*, 5th ed. (Butterworth-Heinemann, 1980).
27. D. H. Ballard, Pattern Recogn. **13**, 111 (1981).
28. M. Lax, J. Appl. Phys. **48**, 3919 (1977).